scientific reports

Check for updates

OPEN

Three-dimensional multicellular layer structure: an advanced *in vitro* model for studying inflammatory bowel diseases

Alice Zaramella[1,2,4], Agner Henrique Dorigo Hochuli[1,2,4], Miriam Duci[1,2], Matteo Marcigaglia[1], Raquel Moll-Diaz[1,2], Paola Bisaccia[1,2], Rudra Kashyap[3], Marcin Jurga[3], Maurizio Muraca[1] & Michela Pozzobon[1,2]✉

Inflammatory Bowel Disease (IBD) is a group of complex and debilitating gastrointestinal disorders characterised by chronic inflammation of the intestinal mucosa. This condition is multifactorial, involving genetic predispositions, environmental influences, dysregulated immune responses, and impaired epithelial barrier function. Researchers have already proposed the use of Extracellular Vesicles (EVs) as a therapeutic approach for inflammatory diseases. EVs are lipid bilayer-delimited nanoparticles secreted by cells that possess anti-inflammatory and pro-regenerative properties. We aim to develop a three-dimensional (3D) multilayer structure (MLS) model that mimics the physiological complexity of the intestinal mucosa, serving as a ready-to-use primary platform for drug testing. MLS, built with Caco-2 cells and BJ fibroblasts, were stimulated with pro-inflammatory cytokines to replicate IBD-like conditions, and within this model, the anti-inflammatory potential of EVs was further investigated. In the MLS, fibroblasts and Caco-2 cells integrated with one another, demonstrating that Caco-2 cells require fibroblasts for assembly. The results obtained from RT-qPCR analysis displayed a significant enhancement in the expression of both pro-inflammatory and anti-inflammatory genes. Specifically, EVs led to an increase in the expression of the *IL-10* anti-inflammatory gene and leucine-rich repeat-containing G protein-coupled receptor 5 (*LGR5*+) stemness gene, suggesting a possible regulatory role of EVs in reducing inflammation and promoting a more balanced immune response. MLSs provide a valuable tool to study the intricate interactions between EVs, epithelial cells, and stromal components, more accurately mimicking native tissue architecture than traditional 2D cultures. The findings contribute to the burgeoning field of 3D models as tools for regenerative medicine applications.

Keywords IBD, 3D culture, Extracellular vesicles, Inflammation

Inflammatory Bowel Disease (IBD) is a group of a complex and multifactorial disorder that significantly impacts the lower Gastrointestinal (GI) tract. IBD mainly includes two different conditions: Crohn's disease (CD) and Ulcerative colitis (UC). IBD is characterised by chronic inflammation, often leading to impaired epithelial barrier function and is associated with intestinal immune dysregulation. The chronic inflammation of the lower GI is promoted by enhanced secretion of pro-inflammatory cytokines such as Interleukin 6 (IL-6), Interleukin 1 beta (IL-1β), and Tumor necrosis factor alpha (TNFα). All of them play a crucial role in the onset of this pathology[1–3]. These pro-inflammatory cytokines are produced by immune cells in response to microbial *stimuli* or tissue damage, contributing to the amplification and perpetuation of intestinal inflammation.

Studying IBD using three-dimensional (3D) culture models, such as 3D multicellular layer structures (MLS), spheroids and organoids, has emerged as a pivotal advancement in the field of GI diseases[4]. Despite being cheap and well-established, two-dimensional (2D) immortalised cell cultures in monolayers do not recapitulate whole organ cell–cell interactions and extracellular microenvironment[5,6]. On the other hand, culturing a heterogeneous pool of intestinal cell types and obtaining immortalised cell lines that secrete mucus to mimic the physiology

[1]Stem Cell and Regenerative Medicine Lab, Institute of Pediatric Research Città Della Speranza, Corso Stati Uniti 4, 35127 Padova, Italy. [2]Department of Women's and Children's Health, University of Padua, Via Giustiniani 2, 35128 Padova, PD, Italy. [3]EXO Biologics, Boulevard de Patience et Beaujonc, 3/2, 4000 Liege, Belgium. [4]Alice Zaramella and Agner Henrique Dorigo Hochuli authors contributed equally to this work. ✉email: michela.pozzobon@unipd.it

of the *in vivo* intestinal barrier can be challenging[7]. In a more realistic scenario, the *in vitro* 3D innovative culture methods offer unique advantages over traditional 2D cell cultures, providing a more physiologically relevant platform to investigate the complex pathogenesis of IBD[4,5]. 3D models, such as organoids, could better mimic organ architecture, but they are time-consuming and expensive[8]. Spheroids, instead, can represent reliable models in different research areas due to their easy handling and rapid growth[9]. However, mono-cellular spheroids may be a too-simplified culturing method, lacking all the other components of the *invivo* organs[10]. MLS, which is composed of two different cell lines, could overcome these limitations[11].

Extracellular Vesicles (EVs) are a peculiar group of membranous nanoparticles that play crucial roles in intercellular communication and the exchange of bioactive molecules[12]. The EVs can be broadly classified into three main types: exosomes, microvesicles, and apoptotic bodies, each with distinct biogenesis pathways and sizes. Exosomes, typically ranging from 30 to 150 nm, originate from the endosomal compartment and are released upon the fusion of multivesicular bodies with the plasma membrane. Microvesicles, with sizes ranging from 100 to 1000 nm, bud directly from the plasma membrane. Apoptotic bodies, the largest of the three, are released during the process of apoptotic cell death[12]. All cell types secrete EVs, and their cargos include various biomolecules such as proteins, lipids, nucleic acids, and microRNAs, which reflect the cellular origin and physiological state of the producing cell[13,14]. Several studies have demonstrated that EVs derived from Mesenchymal Stromal Cells (MSCs) can serve as a therapeutic tool in the repair of tissue injuries associated with various diseases, including IBD[14–20]. It is already well known that the beneficial effects of MSCs are due to their paracrine signalling mediated by EVs released by the cells[14,17].

In the present work, we developed a 3D model called intestinal MLS with epithelial cells and fibroblasts that cross-talk each other and can regenerate following EV administration after inflammatory damage. We demonstrated that MLS is a responsive model for testing new drugs.

Results

Assessment of Caco-2 and BJ Cells for spheroid formation

Although well-known cell lines, Caco-2 and BJ, were characterised with the final aim of creating a 3D model for studying intestinal inflammation. The proliferation of the adherent epithelial Caco-2 cells was evaluated in monolayer culture, highlighting a doubling time of 76.9 h (Supplementary Fig. 1a). Caco-2 cells also expressed the intracellular junction proteins E-Cadherin and Occludin (Fig. 1a). In parallel, the BJ cell line, fibroblasts derived from skin, exhibited a doubling time of 56.3 h (Supplementary Fig. 1b) and a clear expression of α-SMA and Vimentin (Fig. 1b). Nevertheless, Collagen I was expressed only in BJ cells (Fig. 1c). To evaluate cell-to-cell communications, Caco-2 and BJ cells were co-cultured at a 70:30 ratio, respectively. After five days, the cells exhibited interaction while retaining their original morphology and marker expression. (Fig. 1d).

To assess whether Caco-2 and BJ cells can form spheroid-like structures when cultured alone, the cells were seeded in ultra-low attachment plates and monitored for reorganisation and the formation of 3D structures (Fig. 1e, f). After 7 days, Caco-2 cells did not form spheroids. In contrast, BJ cells successfully formed a 3D-like structure, characterised by a dark inner core. However, a balance of Caco-2 and BJ cells in a co-culture may represent a better strategy for obtaining a 3D model that combines the characteristics of Caco-2 (intestinal epithelial barrier) and BJ (Collagen I deposition).

A 3D co-culture of Caco-2 and BJ can form a consistent multicellular layer structure

To develop the MLS free of matrices, we studied the optimal proportion of cells to form the 3D model. Specifically, the cell tracker DiO for Caco-2 cells and Dil for BJ cells were used (Fig. 1g). The 70:30 ratio yielded better distribution, resulting in more distinct and independent spherical structures (Fig. 1g and Supplementary Fig. 2a). This configuration also demonstrated the improved spatial distribution of both Caco-2 and BJ cells compared to the 50:50 MLS condition.

A Live and Dead (L/D) assay was performed on day 6 for both ratios to further evaluate cell viability. As shown in Fig. 1h, MLSs maintained their viability along the experiments, with a significant statistical difference (50:50 *vs.* 70:30, $p = 0.0052$). These findings suggest that the 70:30 ratio is optimal for forming effective 3D structures, with BJ cells contributing to collagen production that remodels the Caco-2 culture into consistent MLS. Indeed, the Collagen I staining confirmed the presence of this protein in the core of MLS (Supplementary Fig. 2b). Given the enhanced cell distribution, morphology and viability, we selected the 70:30 MLS for further investigation.

Defining optimal cytokine dosage for inducing inflammation in the MLS

To establish the best protocol to mimic an inflammatory environment, MLSs were primed with a pro-inflammatory cocktail for 24 h and analysed after 2 days (Fig. 2a). To determine the optimal protocol, the MLSs were stimulated with three different dosages of a pro-inflammatory cytokine cocktail: 25 ng/mL, 50 ng/mL, and 100 ng/mL. The effect of the pro-inflammatory cocktail on the MLS was evaluated through gene expression analysis of intestinal cell markers and inflammation-related genes. Samples treated with 25 ng/mL showed an upregulation of *IL-10* expression ($p = 0.0002$), a downregulation of *MUC5* ($p = 0.0200$) and *OCCLUDIN* ($p = 0.0077$), and no significant changes in *LGR5+*, *MUC2*, *TNFARSF1A,* and *IL-6* genes when compared to no-damaged MLS (Fig. 2b). In samples treated with 50 ng/mL, the pro-inflammatory gene *IL-6* and the anti-inflammatory gene *IL-10* were significantly upregulated ($p = 0.0113$ and $p = 0.0038$, respectively), with no significant changes in *LGR5+*, *MUC2*, *MUC5*, O*CCLUDIN,* and *TNFARSF1A* when compared to the control (Fig. 2b). Conversely, in samples treated with 100 ng/mL, an upregulation of *MUC2* ($p = 0.0042$), *IL-6* ($p = 0.0008$), and *IL-10* ($p = < 0.0001$), along with a downregulation of *OCCLUDIN* ($p = 0.0092$), was observed. No changes in *LGR5+* ($p = 0.1302$), *MUC5* ($p = 0.8476$), and *TNFARSF1A* ($p = 0.1054$) genes were noted when compared with the no-damaged MLS (CTRL) (Fig. 2b). Following these results, the area of MLS on days 3, 4, and 5 was also analysed, considering the 100 ng/mL condition (Fig. 2c, d). After administration of the pro-inflammatory cocktail (Day 4), the area

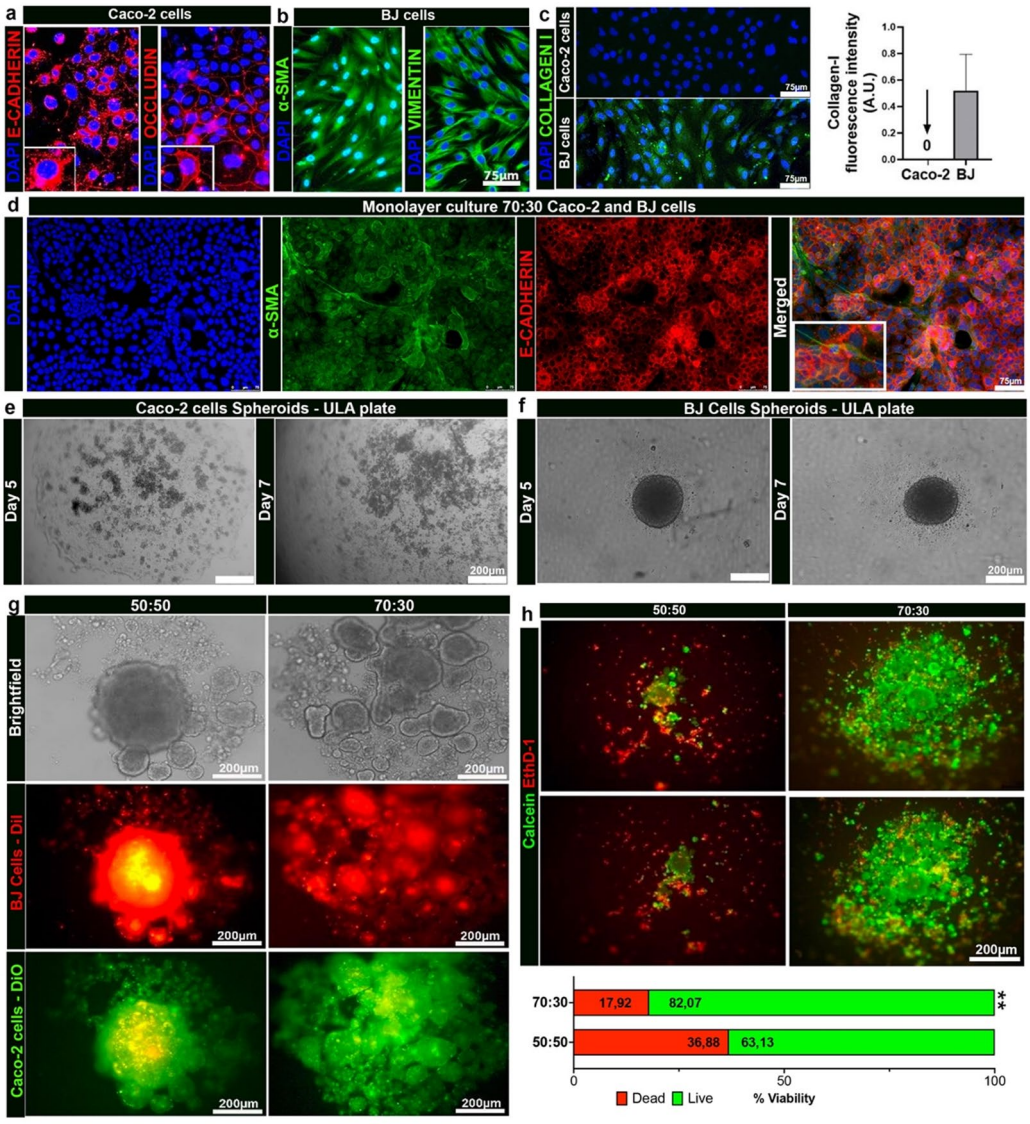

Fig. 1. Caco-2 and BJ cell characterisation, co-culture, and Multicellular Layer Structure (MLS) development. **(a)** Immunofluorescence image of Caco-2 cells stained for E-Cadherin and Occludin, with nuclei (DAPI). Scale bar = 75 µm. **(b)** Immunofluorescence image of BJ cells stained for α-SMA and Vimentin, with nuclei (DAPI). Scale bar = 75 µm. **(c)** Immunofluorescence image of Caco-2 and BJ cells stained for Collagen I, with nuclei (DAPI) and quantification. Scale bar = 75 µm. **(d)** Immunostaining of a monolayer co-culture of Caco-2 and BJ cells at the 70:30 proportion, highlighting the presence of BJ cells stained for α-SMA (green), Caco-2 cells stained for E-cadherin (red), and nuclei (DAPI, blue) (scale bar = 75 µm). **(e–f)** Brightfield images of Caco-2 and BJ cell spheroids, respectively, cultured for 5 and 7 days (scale bar = 200 µm). **(g)** Brightfield and immunofluorescence images of the MLS culture of BJ cells (stained red with Dil dye) and Caco-2 cells (stained green with DiO dye) at 50:50 and 70:30 ratios, captured on day 6 (scale bar = 200 µm). **(h)** Representative images of Live/Dead assay and quantification of the 50:50 and 70:30 MLS ratios, respectively. Live cells are stained in green (calcein), and dead cells in red (ethidium homodimer-1) (scale bar = 200 µm). Statistical analyses were performed using the Student T test and reported as $^{**}p < 0.01$. (n = 6).

of damaged MLS was significantly reduced ($p = 0.0205$) compared to the control (Fig. 2d). The gene expression and morphology analyses indicated that MLS treated with a 100 ng/mL cytokine cocktail responded to the pro-inflammatory *stimulus* by significantly expressing both pro-inflammatory and anti-inflammatory genes, resembling the damage observed in *in vivo* IBD. In contrast, the other tested concentrations were less effective.

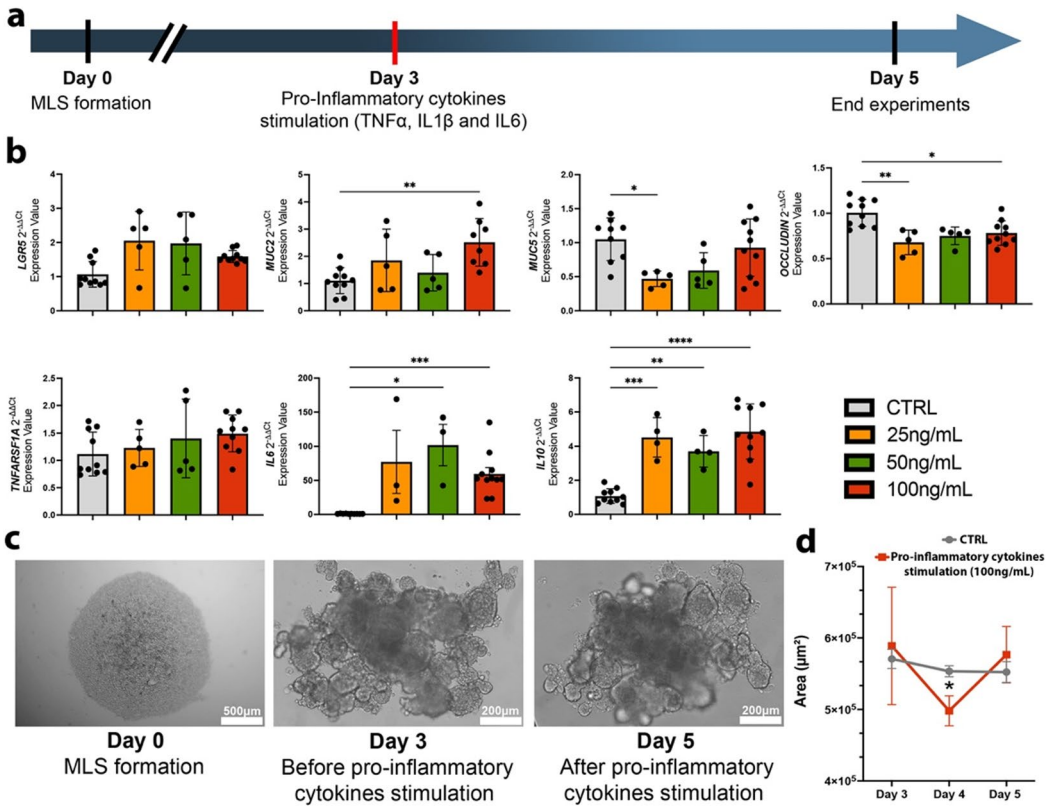

Fig. 2. Setting up of pro-inflammatory cytokines-stimulated damage on Multicellular Layer Structure (MLS). **(a)** The time frame starts with the seeding of MLS in an ultra-low attachment plate (Day 0), followed by cytokine-stimulated damage using a pro-inflammatory cocktail (Day 3) and the collection of samples for analysis (Day 5). **(b)** Comparison of gene expression levels for *LGR5* + , *MUC2*, *MUC5*, *OCCLUDIN*, *TNFARSF1A*, *IL-6*, and *IL-10* in MLS treated with different concentrations of a pro-inflammatory cocktail (25 ng/mL, 50 ng/mL, and 100 ng/mL). Unstimulated MLS (CTRL) was used as a control. $^{*}p < 0.05$; $^{**}p < 0.01$; $^{***}p < 0.001$; $^{****}p < 0.0001$. **(c)** Representative brightfield images during MLS formation (Day 0), prior to (Day 3) and following cytokine-stimulated damage (100 ng/mL) (Day 5). (Scale bar = 500 or 200 µm). **(d)** Area (μm^2) comparison of MLS treated with 100 ng/mL of the pro-inflammatory cocktail and the unstimulated MLS (CTRL). $^{*}p < 0.05$. Statistical analyses were performed using the ANOVA test, n = 4 for area evaluation.

Pro-inflammatory cytokine-stimulated MLS treated with EVs showed an upregulation of regenerative and anti-inflammatory genes

After establishing the optimal dose to induce the pro-inflammatory damage on MLS, we further investigated the effects of EV treatment, using Dexamethasone as a positive control (Fig. 3a). EVs were produced in the Good Manufacturing Practice (GMP) environment.

To correctly classify EV according to the international guidelines[21], their immunophenotypic profile was evaluated. Specifically, the canonical tetraspanins CD9, CD63, and CD81, as well as markers for MSC, immunological factors, and adhesion molecules. The analysis revealed a high presence of the CD9, CD63, and CD81 markers in the EVs, along with an expression of MSC phenotypic markers, particularly CD105 and CD44. Conversely, there was a low expression of SSEA4, HLA-1A, HLA-DR, and CD45. Additionally, the results indicated a high expression of adhesion molecules such as MCSP and CD49e, while immunological markers (CD11c and CD19) were found to be expressed at low levels (Fig. 3b).

The capability of EVs to reduce inflammation was evaluated using the Griess assay. After stimulation with Lipopolysaccharide (LPS) to mimic an inflammatory response, macrophages acquired an M1 phenotype, resulting in increased inducible nitric oxide synthase (iNOS) and nitric oxide (NO) production. Therefore, nitrite concentration serves as an indicator of M1 polarisation. With the administration of EVs, the concentration of NO in culture media was reduced in a dose-dependent manner (Fig. 3c), suggesting their ability to reduce nitrite levels, prevent M1 phenotype acquisition by macrophages, and, in turn, exert an anti-inflammatory effect.

Interestingly, inflammatory cytokine-stimulated MLS showed no drastic morphology difference in samples treated with EVs and Dexamethasone (Fig. 3d). However, the area measurement (Fig. 3e) highlighted a significant increase in cytokine-stimulated MLS treated with EVs when compared with unstimulated MLS (CTRL) ($p = 0.0479$), inflammatory cytokine-stimulated MLS ($p = 0.0466$), and inflammatory cytokine-stimulated MLS treated with Dexamethasone ($p = 0.0143$) (Fig. 3f).

However, treatment with EVs and Dexamethasone revealed significant effects on gene expression in cytokine-stimulated MLS (Fig. 3g). Stimulated MLS treated with EVs exhibited an upregulation of *MUC5*

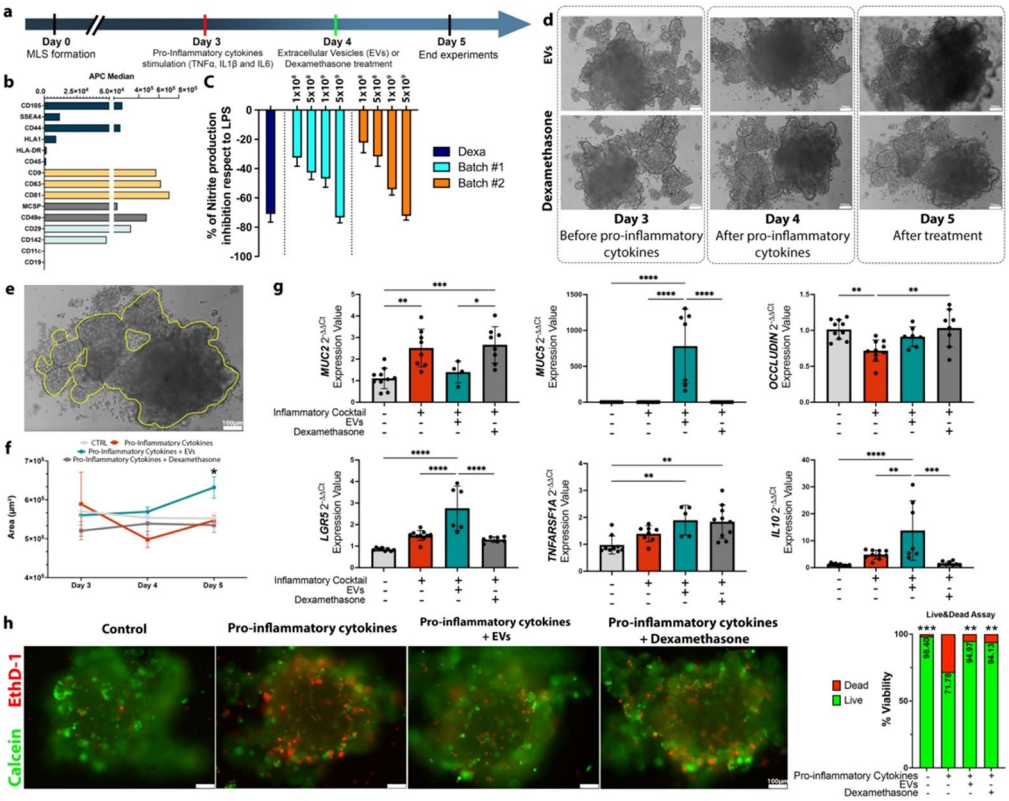

Fig. 3. Analysis of Multicellular Layer Structure (MLS) after Extracellular Vesicles (EVs) and Dexamethasone treatments. **(a)** The timeline starts with the seeding of MLS in an ultra-low attachment plate (Day 0), followed by cytokine stimulation with the pro-inflammatory cocktail (Day 3), treatment with EVs or Dexamethasone (Day 4), and collection of samples for analysis (Day 5). **(b)** Immunophenotypic characterisation of GMP-grade EVs derived from Mesenchymal Stromal Cells. **(c)** Griess Assay results indicating the capability of EVs to reduce nitrite production by macrophages (RAW 264.7). Two different batches of GMP-EVs were tested. Dexamethasone (Dexa) (1 µg/mL) was used as a positive control. The bars represent the percentage reduction in nitrite production due to Dexamethasone (blue bar) and EVs at various concentrations ($1 \times 10\text{^}8$, $5 \times 10\text{^}8$, $1 \times 10\text{^}9$, $5 \times 10\text{^}9$ particles/ml). Data are shown as mean ± standard deviation. **(d)** Brightfield representative images of MLS during formation (Day 3, before cytokine stimulation), after cytokine stimulation (Day 4), and post-treatment with EVs or Dexamethasone (Day 5). (Scale bar = 100 µm). **(e)** Representative images of the manual area counting method using the digital pen. **(f)** Area (µm^2) comparison of MLS stimulated with pro-inflammatory cytokines (100 ng/mL) and treated with EVs or Dexamethasone. The Student t Test was used for statistical analyses and is reported as $^*p < 0.05$. n = 4 for area evaluation. **(g)** Comparison of gene expression levels for *MUC2*, *MUC5*, *OCCLUDIN*, *LGR5+*, *TNFARS1A*, and *IL-10* in MLS treated with a pro-inflammatory cocktail (100 ng/mL) against those treated with EVs or Dexamethasone. Untreated and non-stimulated MLS (CTRL) were used as controls. Statistical analyses were performed using the ANOVA test. $^*p < 0.05$; $^{**}p < 0.01$; $^{***}p < 0.001$; $^{****}p < 0.0001$. **(h)** Live and Dead assay of MLS in control, after cytokine stimulation, and cytokine-stimulated MLS treated with EVs or Dexamethasone. On the left, representative images of live cells are stained green (calcein), and dead cells red (ethidium homodimer-1). (Scale bar = 100 µm). On the right, the quantification of live and dead cells. Statistical analysis was performed with the ANOVA test. $^{**}p < 0.01$; $^{***}p < 0.001$.

($p < 0.0001$), *LGR5+* ($p = 0.0001$), and *IL-10* ($p = 0.0055$) compared to untreated cytokine-stimulated MLS. Interestingly, *TNFARSF1A* showed an upregulation when compared to non-damaged MLS ($p = 0.0148$) and an upregulation of *LGR5+* ($p < 0.0001$) relative to Dexamethasone. These results support the regenerative and anti-inflammatory potential of EVs in response to a stressed environment, stimulating the proliferation of *LGR5+* cells (stem cells). Moreover, cytokine-stimulated MLS treated with Dexamethasone demonstrated the expected anti-inflammatory effect but failed to show any regenerative impact, as no significant changes in *LGR5+* expression were observed compared to both undamaged MLS ($p = 0.7060$) and cytokine-stimulated MLS ($p = 0.8565$). Notably, a significant downregulation of *LGR5+* expression ($p < 0.0001$) was identified when compared to EV-treated samples. Additionally, a significant downregulation in *MUC5* ($p < 0.0001$) and *IL-10* ($p = 0.0002$) expression levels was noted. Finally, the viability of MLS during the experiment was evaluated. A higher number of dead cells was observed in cytokine-stimulated MLS compared to the other groups, as shown in Fig. 3h. The presence of E-cadherin following cytokine administration and after treatment with EVs or

Dexamethasone was also assessed by immunofluorescence. The protein was consistently found in all conditions, indicating that all groups continued to express adherent junctions (Supplementary Fig. 2c).

Discussion

IBD, including Crohn's disease and ulcerative colitis, continue to rise in incidence across Europe, reaching up to 22.8 and 44.0 cases per 100,000 person-years, respectively[22]. Despite therapeutic advances, current treatment options, ranging from immunosuppressants to biological agents, are associated with other significant side effects[23]. Thus,there is a clinical need to test new drugs and explore innovative pharmacological approaches.

In this work, we developed and characterised a human cell-based 3D *in vitro* model free from commercial matrices. The main advantages of this model are based on (1) the short culture period, (2) the cross-talk between the two cell populations that form the intestine, such as the epithelial cells and fibroblasts, and (3) their ability to be responsive after a pro-inflammatory damage.

Several *in vitro* models have been developed to replicate the intestinal environment, each with specific advantages and limitations. Organoids, derived from stem cells, represent a gold standard for recapitulating epithelial architecture and have been successfully used to model intestinal development, disease, and drug response[24–28]. However, they require complex protocols, expensive matrices (e.g., Matrigel), and are subject to batch-to-batch variability[29,30].

At the opposite end, simpler models, such as the scaffold-free epithelial spheroids described by Gheytanchi et al.[31], offer cost-effectiveness and reproducibility but lack the stromal compartment, which is critical for mimicking *in vivo* cell–cell interactions. More complex co-culture systems have also been proposed, often using transwell inserts and artificial scaffolds[32], but these can introduce technical variability and lack physiological self-assembly.

However, our MLS model, which includes intestinal epithelial cells and fibroblasts that self-assemble into a 3D structure, offers several advantages over transwell-based systems, providing a balance between physiological relevance and experimental manageability. By co-culturing epithelial (Caco-2) and fibroblast cells in low-attachment conditions, we achieved spontaneous 3D self-assembly without the need for exogenous scaffolds. This architecture enables natural stromal-epithelial interactions, which are essential for tissue organisation and inflammatory responses. Unlike transwell-based models, MLS form compact spheroids with intrinsic spatial patterning, potentially reducing variability while enhancing biological relevance.

A relevant comparison may be made with the co-culture models developed by Darling et al.[33], who engineered three-dimensional constructs in which Caco-2 epithelial cells were cultivated on fibroblast-derived stromal compartments. Their research emphasised that direct epithelial–stromal contact significantly enhances epithelial polarization, facilitates the formation of basement membrane-like structures, and decreases transepithelial electrical resistance to levels more closely resembling those of the human intestine, thereby augmenting the physiological relevance of drug permeability studies. In contrast, our MLS offers a rapid and scaffold-free system in which epithelial and fibroblast cells self-assemble into compact spheroids that not only preserve barrier-associated markers but also actively respond to inflammatory cytokines. While Darling et al.[33] mainly focused on barrier architecture and absorption properties, our MLS was specifically challenged by a pro-inflammatory microenvironment, recreating disease-relevant features of IBD such as tight junction disruption and altered mucin expression. Importantly, our model enabled the evaluation of extracellular vesicle therapy, demonstrating regenerative and anti-inflammatory responses through the upregulation of *IL-10* and *LGR5* + stemness markers. Therefore, whereas the Darling and colleagues[33] model highlights epithelial fidelity for pharmacokinetic studies, our MLS broadens the application of fibroblast–epithelial co-culture towards modelling intestinal inflammation and therapeutic intervention, thus providing a complementary platform for both mechanistic studies and preclinical drug testing.

We focused on recapitulating the colon epithelial barrier, along with the surrounding stroma cells, a mixture shown to be responsive to injury and capable of reorganising toward a recovery-oriented conformation following damage. Caco-2 cell line, which expresses the stem cell marker LGR5[34,35], is widely employed in preclinical research, including drug permeability, solubility, and nanoparticle translocation studies. Furthermore, it is recognised by the U.S. Food and Drug Administration (FDA) as a reliable model for supporting new drug applications[36] . The BJ primary fibroblast cell line has created the stromal layer, which functions well as an adherent element in colon tissue.

The pro-inflammatory cytokine cocktail used to induce damage in MLS mimicking the inflammatory microenvironment characteristic of IBD was carefully selected for its synergistic action in an inflammatory context[37,38]. In tissue, the inflammatory microenvironment facilitates the infiltration of immune cells into the intestinal mucosa, leading to aberrant wound-healing responses and tissue disruption. The latter is also recapitulated in our model.

IL-6 is a pro-inflammatory cytokine that plays a crucial role in managing immune responses and inflammation. Binding to its receptor (IL-6 receptor) induces an acute phase response, triggering downstream signalling cascades and the transcription of many pro-inflammatory genes[1]. IL-1β is a potent pro-inflammatory cytokine crucial in initiating and maintaining inflammatory and immune responses[2]. TNFα is one of the primary mediators of gut inflammation in IBD pathogenesis[3]. It is mainly produced by immune cells such as macrophages, monocytes, and T cells in response to various *stimuli*, including infection, tissue injury, and immune challenges. Inflammation-promoting actions of TNFα induce vasodilation, increasing vascular permeability and attracting immune cells to the site of inflammation[3]. This study demonstrated that MLS consistently respond to damage in a reproducible manner, exhibiting a clear dose-dependent response. After cytokine administration, a substantial perturbation of the model was observed. The primary disruption centred around the intestinal epithelial barrier, which is characterised by the loss of tight junctions. Moreover, we demonstrate that after 24 h of culturing MLS

with the pro-inflammatory cocktail, MLS can respond to the inflammatory environment, upregulating *MUC2*, *OCCLUDIN* and *IL-10* genes.

Following pro-inflammatory stimulation, the therapeutic treatment was evaluated through the administration of EVs. The strategic use of EVs as potential therapeutic agents in the inflammatory intestinal models represents the second focus of the project. Our research group has already demonstrated the anti-inflammatory efficacy of EVs *in vivo* in skeletal muscle[39], in the colitis environment[20] and in pediatric lung disease[19]. Building on these promising findings, the current study focuses on extending the application of these EVs to an *in vitro* human cytokine-stimulated model of intestinal inflammation. The GMP-EV dosages were selected based on their demonstrated efficacy in previous studies, where their properties were extensively characterised[39]. These EVs exhibited an immunophenotypic profile characteristic of nanoparticles, confirming their origin and the potential to evade immune recognition, as indicated by the absence of HLA-DR expression[40]. Following EV administration on the cytokine-stimulated MLS, an upregulation of *LGR5+*, *MUC5*, *TNFARSF1A*, and *IL-10* genes was observed. LGR5+, consistently present in Caco-2 cells and absent in BJ, are well-known as intestinal stem cells responsible for regenerating various cell types within the crypt compartment[41–43]. The observed upregulation of *LGR5+* expression following EV treatment suggests that EVs may stimulate this stem cell population, potentially enhancing the regenerative process within the intestinal epithelium. Although *TNFARSF1A* is generally known for mediating TNF-α signalling, its upregulation in our model occurred along with the increased *IL-10* expression. This could suggest a potential regulatory or anti-inflammatory adaptation, rather than an exacerbation of inflammation. *TNFARSF1A* is, in fact, also known to be involved in homeostatic processes such as epithelial repair and resolution of inflammation under certain conditions, including IBD[44,45]. It is well established that the cargo of EVs can influence the damaged environment by delivering signals that promote tissue repair[46,47]. In our case, we hypothesise that microRNAs carried within the EVs play a key role in regulating gene expression to promote the upregulation of anti-inflammatory genes. Ongoing experiments aim to further characterise the EV cargo and investigate its role in MLSs damage repair.

In contrast, samples treated with Dexamethasone did not exhibit any changes in *LGR5+* expression, which aligns with the expected effects of this drug. As a widely used anti-inflammatory treatment, Dexamethasone primarily targets inflammation rather than promoting tissue regeneration[48].

As a whole, the MLS model we proposed has certain limitations. In particular, we developed a 3D structure that mimics intestinal physiology using both intestinal and non-intestinal cell lines. Future implementation of the model will incorporate intestinal fibroblasts. Moreover, the physiological complexity will be improved with other cell types, such as goblet, immune, and endothelial cells. Nonetheless, this model also has significant strengths, including its straightforward protocol, which requires less laboratory material, and its rapid development, allowing for different read-outs within just a week. Moreover, the absence of a 3D commercial matrix, which is mandatory for organoids, makes our model more cost-effective and simpler than organoids.

The findings from this study provide new insights into exploring the therapeutic potential of EVs within our 3D MLS model, particularly in the context of IBD.

Conclusion

In this work, we developed and characterised an in vitro human 3D model free of commercial matrix, which is quick to culture (6 days) and could serve as a rapid and reliable model to mimic the inflammatory condition observed in IBD. The model we described can significantly advance efforts to understand IBD pathophysiology while providing a simple and reproducible tool for investigating therapeutic interventions using EVs. EVs induced an anti-inflammatory response in pro-inflammatory cytokine-stimulated MLS. The up-regulation of pro-regenerative genes (*LGR5+*, *MUC5,* and *IL-10*), increased size of MLS, as well as cell viability, suggests a paramount role of EVs towards the restoration to a physiological state.

Methods

The study was carried out in the Laboratory of Stem Cells and Regenerative Medicine of the Department of Women's and Children's Health, University of Padua, at the Institute of Paediatric Research, Fondazione Città della Speranza.

Monolayer cultures

The human Caco-2 and human fibroblast BJ were used to develop MLS. Caco-2 cell lines were purchased from Creative Bioarray Ltd. and cultured in Dulbecco's modified Eagle's medium (DMEM)/High glucose medium (Gibco) supplemented with 1% of Penicillin–Streptomycin (P/S), 1% of L-Glutamine (Euroclone), 10% of fetal bovine serum (FBS, Gibco) and 1% of Hepes solution 1 M (Gibco). The BJ cell line (Sigma Aldrich) was cultured in a DMEM High glucose supplemented with 1% P/S, 1% L-Glutamine and 10% FBS. Both cell lines were cultured under standard conditions. The complete list of reagents with the corresponding catalogue number is reported in Supplementary Table 1.

Co-culture of Caco-2 and BJ

To perform the co-culture, Caco-2 and BJ cells were plated on a tissue culture 24-well plate (Corning) 10,000 cells/well in a ratio of 70:30 respectively, and seeded in the MLS culture medium (DMEM/F12, P/S, L-Glutamine, 20 ng/ml of Epidermal Growth Factor (EGF]) 10 ng/ml of Basic Fibroblast Growth Factor (FGF2) and 2% B-27). To assess the proliferation and growth rates of the Caco-2 and BJ cell lines, 10,000 cells/well were seeded separately into 24-well plates and cultured for 6 days (120 h). Brightfield images were captured daily, and cell counts (n = 4) were determined using in a Bürker Chamber. The growth curve was generated by plotting the

cell numbers over time, with data represented as the average. The doubling time was calculated following the equation[49]:

$$Dt = \frac{ln2}{\frac{\ln(N)-\ln(No)}{t}}$$

A total of three experiments were performed.

Single Caco-2 and BJ spheroid development

To evaluate the spontaneous capacity of Caco-2 and BJ cells to form spheroids, single-cell suspensions (10,000 cells/well) were seeded into their respective culture media in 96-well ultra-low attachment (ULA) plates and centrifuged at 300 g for 5 min. The cells were incubated for 6 days, and brightfield images were captured using the inverted microscope Olympus IX71 to monitor and assess the progression of spheroid formation.

Multicellular-Layer structure

MLSs were developed with the free-floating spheroid culture technique. Single cells (10,000 cells/well) were seeded on a 96-well ULA plate in different ratios: 50:50 and 70:30 of Caco-2 and BJ, respectively. Cells were seeded in MLS culture medium. After seeding without matrix support, the plate was centrifuged for 5 min at 300 *g* to concentrate the cells on the bottom to induce a round shape. MLSs were incubated for 72 h at 37 °C and 5% CO_2. MLSs were monitored on Day 0, Day 3, Day 5, Day 9, and Day 12 (Olympus IX71). The area of the 3D structures was measured using brightfield images of MLS (Fiji software IJ 1.54f. version, NIH, USA). The entire shape of the MLS was traced with a digital pen.

Cell distribution and viability assay on MLS

To gain a deeper understanding of the morphological arrangement of Caco-2 and BJ cells within the MLS structure, Caco-2 cells were labelled with Vybrant DiO dye (Invitrogen) and BJ cells were labelled with Vybrant Dil (Invitrogen). The labelling procedure was performed following the manufacturer's instructions. Labelled MLS seeded in 50:50 and 70:30 ratios were analysed on days 3, 5, 9, and 12. The fluorescence was evaluated using a Leica B5000 inverted microscope.

To evaluate the cell viability of MLS cultured in different ratios, the LIVE/DEAD™ Viability/Cytotoxicity Kit (Invitrogen) was used according to the manufacturer's instructions. Briefly, MLS were stained with calcein-AM and ethidium homodimer-1 and incubated for 30 min at room temperature (RT) in the dark. Images were captured using a Leica B5000 inverted microscope.

Stimulation of MLS with pro-inflammatory cytokines

To simulate IBD, in particular the typical inflammatory environment studied in this model, a pro-inflammatory cocktail including recombinant human IL-1β protein (PeproTech), recombinant human IL-6 protein (PeproTech), and recombinant human TNFα variant protein (PeproTech) was used as previously reported[50]. After 3 days of culture under standard conditions, cytokine stimulation was performed by administering different concentrations of the pro-inflammatory cytokines, including 25 ng/mL, 50 ng/mL, and 100 ng/mL each for 24 h.

Extracellular vesicles

EVs derived from MSCs isolated from the human Wharton's Jelly of cord tissue were produced in accordance with GMP standards and supplied by EXO Biologics (Liège, Belgium). The cord tissues were provided by certified biobanks (Biothèque Hospitalo-Universitaire de Liège and UZA in Antwerpen) registered with the Belgian Federal Agency for Medicines and Health Products, following Belgian law. Detailed protocols for this procedure are outlined in Bisaccia et al.[39]. The size and concentration of the EVs were determined using Nano Tracking Analysis (NTA). For this study, the MACSPlex exosome kit (Miltenyi Biotech) was utilised to identify surface antigen markers, including canonical tetraspanins of EVs, CD9, CD63, and CD81.

MLS treatments

Twenty-four hours after stimulation with the pro-inflammatory cytokines, MLSs were treated with GMP-grade EVs at a dose of 1 × 10^9 particles for 24 h. Dexamethasone was used as a positive control.

Griess assay

The evaluation of EV anti-inflammatory activity was assessed by their capacity to prevent the acquisition of the M1 phenotype in LPS-stimulated RAW 264.7 (Thermo Fisher) macrophages. We measured M1 polarisation by quantifying NO production, following the protocol established by Malvicini et al.[40]. Briefly, RAW 264.7 were seeded in a 96-well plate at a density of 2 × 10^4 cells/well in 120 µL of culture medium. After 24 h, macrophages were stimulated for 16 h with LPS (10 ng/mL) alongside the administration of different doses of EVs (1 × 10^8, 5 × 10^8, 1 × 10^9, 5 × 10^9 particles/mL). As an internal control for the inhibition of M1 polarisation, we used Dexamethasone (1 µg/mL). Cell culture supernatants for each condition were collected to measure NO production. The Griess reaction reagent[51] was added to the cell culture supernatant and incubated for 10 min at RT. The absorbance was measured at 540 nm and compared with a sodium nitrite standard curve (0–50 µM).

Immunofluorescence staining

Monolayers and MLS cultures were fixed with 4% paraformaldehyde (PFA) for 20 min at room temperature (RT) and rinsed with PBS + 0.05% Tween 20. After permeabilisation (PBS + 1% bovine serum albumin (BSA) + 0.5% Triton for 5 min for 2D cells and 1 h for 3D cells), cells were rinsed three times, 5 min each, with the wash

Antibodies	Dilution	Incubation condition
Mouse anti-α-Actin (Sigma-Aldrich, Saint Louis, USA)	1:100	O.N. at 4 °C
Rabbit anti-alpha smooth muscle (Abcam, Cambridge, UK)	1:100	O.N at 4 °C
Rabbit anti-Vimentin (Abcam, Cambridge, UK)	1:100	O.N at 4 °C
Mouse anti-Occludin Monoclonal Antibody (Invitrogen, USA)	1:100	O.N at 4 °C
Mouse anti-E-cadherin (Santa Cruz Biotechnology, Dallas, USA)	1:100	O.N at 4 °C
Rabbit anti-collagen I (Abcam, Cambridge, UK)	1:100	O.N at 4 °C
Goat anti-Mouse IgG Secondary Antibody, Alexa Fluor 488 (Invitrogen, Carlsbad, USA)	1:200	1 h at RT
Goat anti-Mouse IgG Secondary Antibody, Alexa Fluor 594 (Invitrogen, Carlsbad, USA)	1:200	1 h at RT
Chicken anti-Rabbit IgG Secondary Antibody, Alexa Fluor 488 (Invitrogen, Carlsbad, USA)	1:200	1 h at RT
Chicken anti-Rabbit IgG Secondary Antibody, Alexa Fluor 594 (Invitrogen, Carlsbad, USA)	1:200	1 h at RT
DAPI (Invitrogen, Carlsbad, USA)	1:5000	10 min RT

Table 1. Primary and secondary antibodies used for immunofluorescence analysis. O.N.: overnight, RT stand for room temperature. DAPI is 4',6-diamidin-2-fenilindolo.

Gene	Accession number	Primer forward	Primer reverse	Amplicon size
GAPDH	NM_001256799.3	TCCTCTGACTTCAACAGCGA	GGGTCTTACTCCTTGGAGGC	167
LGR5+	NM_003667.4	AGGTCTGGTGTGTTGCTGAG	GTGAAGACGCTGAGGTTGGA	128
MUC2	NM_002457.5	ACTCTCCACACCCAGCATCATC	GTGTCTCCGTATGTGCCGTTGT	132
MUC5	NM_001304359.2	GGTCCTCATTCAGCAGAGCA	GGTGTCAGCTTGGTGTTGTG	195
TNFARSF1A	NM_001346092.2	CCCAAATGGGGGAGTGAGAG	CCAGGAGCACCAGTGGC	85
IL-6	NM_000600.5	CCTTCTCCACAAACATGTAACAAG	TCACCAGGCAAGTCTCCTCA	142
IL-10	NM_000572.3	GCCAAGCCTTGTCTGAGATG	GAGTTCACATGCGCCTTGAT	94

Table 2. Primers used for mRNA qRT-PCR.

solution (PBS + 0.05% Tween 20). Primary antibodies were diluted (as detailed in Table 1) in a blocking buffer (PBS + 1% BSA) and incubated overnight at 4°C. The secondary antibodies were applied as reported in Table 1. Nuclei were stained using DAPI (Sigma-Aldrich) at a dilution of 1:5000. Immunofluorescence images were obtained with a Leica B5000 inverted microscope.

Gene expression

The total RNA was extracted from MLS using the TRIzol reagent (Invitrogen), and 1 µg of RNA was used for cDNA synthesis with the High-Capacity Kit (Applied Biosystems) according to the manufacturer's instructions. The cDNA (5 ng/µL) was used to perform a Real-Time Polymerase Chain Reaction (RT-qPCR) using SYBR green (Applied Biosystems) for the markers of intestinal cells: *LGR5+*, *MUC2*, *MUC5, OCCLUDIN*, as well as pro-inflammatory and anti-inflammatory markers: TNF receptor superfamily member 1A (*TNFRSF1A*), *Interleukin* 6, *Interleukin* 10, and the housekeeping gene Glyceraldehyde-3-phosphate dehydrogenase (*GAPDH*). The primer sequences and additional details are listed in Table 2. The $2^{-\Delta\Delta Ct}$ method was used for data quantification.

Statistical analysis

All data were processed and statistical significance was determined using GraphPad Prism software version 9.0.0 for macOS (USA). Data are represented as mean (±), standard error of the mean (SEM), or standard deviation (SD). For all experiments, normality and lognormality were assessed using the Shapiro–Wilk test. For the two-group comparison, Student's t-test was performed for normally distributed data, while the Mann–Whitney U test was used for non-parametric data. For comparisons between more than two groups, the one-way ANOVA test was used for normally distributed data, followed by post-hoc testing (with Tukey's test correction). For non-parametric data, the Kruskal–Wallis test was utilised, followed by Dunn's post-hoc test. For gene expression analyses, 6 to ten replicates were performed. The "Identify Outliers" function with the ROUT methods was used to eliminate outlier values. Statistical significance was indicated as follows: $p \geq 0.05$ (ns), $p < 0.05$ (*), $p < 0.01$ (**), $p < 0.001$ (***), and $p < 0.0001$ (****).

Data availability

The materials are already available in the manuscript. Raw data are available under reasonable request to michela.pozzobon@unipd.it.

Received: 18 May 2025; Accepted: 14 October 2025
Published online: 19 November 2025

References

1. Tanaka, T., Narazaki, M. & Kishimoto, T. Il-6 in inflammation, Immunity, and disease. *Cold Spring Harb Perspect. Biol.* **6**, a016295 (2014).
2. Dinarello, C. A. Overview of the IL-1 family in innate inflammation and acquired immunity. *Immunol. Rev.* **281**, 8–27. https://doi.org/10.1111/imr.12621 (2018).
3. Kalliolias, G. D. & Ivashkiv, L. B. TNF biology, pathogenic mechanisms and emerging therapeutic strategies. *Nat. Rev. Rheumatol.* **12**, 49–62 (2016).
4. Duci, M. et al. Research models to mimic necrotizing enterocolitis and inflammatory bowel diseases: Focus on extracellular vesicles action. *Stem Cells* https://doi.org/10.1093/stmcls/sxad068 (2023).
5. O'Connell, L., Winter, D. C. & Aherne, C. M. The role of organoids as a novel platform for modeling of inflammatory bowel disease. *Front. Pediatr.* **9**, 624045 (2021).
6. Gjorevski, N. et al. Designer matrices for intestinal stem cell and organoid culture. *Nature* **539**(7630), 560–564 (2016).
7. Dotti, I. & Salas, A. Potential use of human stem cell-derived intestinal organoids to study inflammatory bowel diseases. *Inflamm. Bowel Dis.* **24**, 2501–2509 (2018).
8. Mollaki, V. Ethical challenges in organoid use. *Biotech* **10**, 12 (2021).
9. Gilazieva, Z., Ponomarev, A., Rutland, C., Rizvanov, A. & Solovyeva, V. Promising applications of tumor spheroids and organoids for personalized medicine. *Cancers* **12**, 2727 (2020).
10. Białkowska, K., Komorowski, P., Bryszewska, M. & Miłowska, K. Spheroids as a type of three-dimensional cell cultures—Examples of methods of preparation and the most important application. *Int. J. Mol. Sci.* **21**, 6225 (2020).
11. Han, S. J., Kwon, S. & Kim, K. S. Challenges of applying multicellular tumor spheroids in preclinical phase. *Cancer Cell. Int.* **21**, 152 (2021).
12. Raposo, G. & Stoorvogel, W. Extracellular vesicles: Exosomes, microvesicles, and friends. *J. Cell Biol.* **200**, 373–383. https://doi.org/10.1083/jcb.201211138 (2013).
13. Colombo, M., Raposo, G. & Théry, C. Biogenesis, secretion, and intercellular interactions of exosomes and other extracellular vesicles. *Annu. Rev. Cell Dev. Biol.* **30**, 255–289. https://doi.org/10.1146/annurev-cellbio-101512-122326 (2014).
14. Mao, F. et al. Exosomes derived from human umbilical cord mesenchymal stem cells relieve inflammatory bowel disease in mice. *Biomed. Res. Int.* **2017**, 5356760 (2017).
15. Zhou, Y. et al. Exosomes released by human umbilical cord mesenchymal stem cells protect against cisplatin-induced renal oxidative stress and apoptosis in vivo and in vitro. *Stem Cell Res. Ther.* **4**, 1–13 (2013).
16. Li, T. *et al.* Exosomes Derived from Human Umbilical Cord Mesenchymal Stem Cells Alleviate Liver Fibrosis. https://home.liebertpub.com/scd **22,** 845–854 (2012).
17. Sicco, C. L. et al. Mesenchymal stem cell-derived extracellular vesicles as mediators of anti-inflammatory effects: Endorsement of macrophage polarization. *Stem Cells Transl. Med.* **6**, 1018–1028 (2017).
18. Jiang, X. et al. Extracellular vesicles derived from human ESC–MSCs target macrophage and promote anti-inflammation process, angiogenesis, and functional recovery in ACS-induced severe skeletal muscle injury. *Stem Cell Res. Ther.* **14**, 1–21 (2023).
19. Bisaccia, P. et al. Extracellular vesicles from mesenchymal umbilical cord cells exert protection against oxidative stress and fibrosis in a rat model of bronchopulmonary dysplasia. *Stem Cells Transl. Med.* **13**, 43 (2023).
20. Tolomeo, A. M. et al. Extracellular vesicles secreted by mesenchymal stromal cells exert opposite effects to their cells of origin in murine sodium dextran sulfate-induced colitis. *Front. Immunol.* **12**, 627605–627620 (2021).
21. Welsh, J. A. et al. Minimal information for studies of extracellular vesicles (MISEV2023): From basic to advanced approaches. *J. Extracell Vesicles 13*, 1–84 (2024).
22. Zhao, M., Gönczi, L., Lakatos, P. L. & Burisch, J. The burden of inflammatory bowel disease in Europe in 2020. *J. Crohns Colitis* **15**, 1573–1587 (2021).
23. Vieujean, S. et al. Understanding the therapeutic toolkit for inflammatory bowel disease. *Nat. Rev. Gastroenterol. Hepatol.* **2025**, 1–24. https://doi.org/10.1038/s41575-024-01035-7 (2025).
24. Sarvestani, S. K. et al. Induced organoids derived from patients with ulcerative colitis recapitulate colitic reactivity. *Nat. Commun.* **12**, 262 (2021).
25. Zachos, N. C. et al. Human enteroids/colonoids and intestinal organoids functionally recapitulate normal intestinal physiology and pathophysiology. *J. Biol. Chem.* **291**, 3759–3766 (2016).
26. Hou, Q. et al. Lactobacillus accelerates ISCs regeneration to protect the integrity of intestinal mucosa through activation of STAT3 signaling pathway induced by LPLs secretion of IL-22. *Cell Death Differ.* **25**, 1657–1670 (2018).
27. Baker, E. J. et al. Advancing nonclinical innovation and safety in pharmaceutical testing. *Drug Discov. Today* **24**, 624–628 (2019).
28. Mochel, J. P. et al. Intestinal stem cells to advance drug development, precision, and regenerative medicine: A paradigm shift in translational research. *AAPS J.* **20**, 17 (2018).
29. Tian, C. M. et al. Stem cell-derived intestinal organoids: A novel modality for IBD. *Cell Death Discov.* **9**(1), 16 (2023).
30. Wang, H., Li, X., You, X. & Zhao, G. Harnessing the power of artificial intelligence for human living organoid research. *Bioact. Mater.* **42**, 140–164. https://doi.org/10.1016/j.bioactmat.2024.08.027 (2024).
31. Gheytanchi, E. et al. Morphological and molecular characteristics of spheroid formation in HT-29 and Caco-2 colorectal cancer cell lines. *Cancer Cell Int.* **21**, 204-216 (2021).
32. Ferreira, B. et al. Establishment of a 3D multi-layered in vitro model of inflammatory bowel disease. *J. Control. Release* **377**, 675–688 (2025).
33. Darling, N. J., Mobbs, C. L., González-Hau, A. L., Freer, M. & Przyborski, S. Bioengineering novel in vitro Co-culture models that represent the human intestinal mucosa with improved Caco-2 structure and barrier function. *Front. Bioeng. Biotechnol.* **8**, 992–1007 (2020).
34. He, S. et al. Expression of Lgr5, a marker of intestinal stem cells, in colorectal cancer and its clinicopathological significance. *Biomed. Pharmacother.* **68**, 507–513 (2014).
35. Alharbi, S. A., Ovchinnikov, D. A. & Wolvetang, E. Leucine-rich repeat-containing G protein-coupled receptor 5 marks different cancer stem cell compartments in human Caco-2 and LoVo colon cancer lines. *World J. Gastroenterol.* **27**, 1578–1594 (2021).
36. Larregieu, C. A. & Benet, L. Z. Drug discovery and regulatory considerations for improving in silico and in vitro predictions that use caco-2 as a surrogate for human intestinal permeability measurements. *AAPS J.* **15**, 483–497 (2013).
37. Macedo, M. H., Dias Neto, M., Pastrana, L., Gonçalves, C. & Xavier, M. Recent advances in cell-based in vitro models to recreate human intestinal inflammation. *Adv. Sci.* **10**, 2301391 (2023).
38. Joshi, A., Soni, A. & Acharya, S. In vitro models and ex vivo systems used in inflammatory bowel disease. *In vitro models* **1**, 213–227 (2022).
39. Magarotto, F. et al. Muscle functional recovery is driven by extracellular vesicles combined with muscle extracellular matrix in a volumetric muscle loss murine model. *Biomaterials* **269**, 120653–120668 (2021).
40. Malvicini, R. et al. Macrophage bioassay standardization to assess the anti-inflammatory activity of mesenchymal stromal cell-derived small extracellular vesicles. *Cytotherapy* **24**, 999–1012 (2022).
41. Sato, T. et al. Single Lgr5 stem cells build crypt-villus structures in vitro without a mesenchymal niche. *Nature* **459**, 262–265 (2009).
42. Wang, Z., Qu, Y.-J., Cui, M., Chief Physician, A. & Professor, A. Modulation of stem cell fate in intestinal homeostasis, injury and repair. *World J. Stem Cells* **15**, 354 (2023).

43. Zheng, L. & Duan, S. L. Molecular regulation mechanism of intestinal stem cells in mucosal injury and repair in ulcerative colitis. *World J. Gastroenterol.* **29**, 2380 (2023).
44. Sedger, L. M. & McDermott, M. F. TNF and TNF-receptors: From mediators of cell death and inflammation to therapeutic giants—Past, present and future. *Cytokine Growth Factor Rev.* **25**, 453–472 (2014).
45. Ruder, B., Atreya, R. & Becker, C. Tumour necrosis factor alpha in intestinal homeostasis and gut related diseases. *Int. J. Mol. Sci.* **20**, 1887 (2019).
46. Berumen Sánchez, G., Bunn, K. E., Pua, H. H. & Rafat, M. Extracellular vesicles: mediators of intercellular communication in tissue injury and disease. *Cell Commun. Signal.* **19**, 1–18 (2021).
47. Roefs, M. T., Sluijter, J. P. G. & Vader, P. Extracellular vesicle-associated proteins in tissue repair. *Trends Cell Biol.* **30**, 990–1013 (2020).
48. Dong, K. et al. Dexamethasone-loaded lipid calcium phosphate nanoparticles treat experimental colitis by regulating macrophage polarization in inflammatory sites. *Int. J. Nanomed.* **19**, 993–1016 (2024).
49. Freshney, R. I. *Culture of Animal Cells* (Wiley, 2010). https://doi.org/10.1002/9780470649367.
50. d'Aldebert, E. et al. Characterization of human colon organoids from inflammatory bowel disease patients. *Front. Cell Dev. Biol.* **8**, 363–376 (2020).
51. Green, L. C. et al. Analysis of nitrate, nitrite, and [15N]nitrate in biological fluids. *Anal. Biochem.* **126**, 131–138 (1982).

Acknowledgements

We thank Domenico Mancuso, Elisabetta Gramegna, Dimitri Stevens, and Ruben Hermans from EXO Biologics for their assistance in producing and characterising EVs, and Gabrielis Kundrotas from EXO Biologics for reviewing the manuscript. We also thank Matteo Marin for his efforts in producing the MLS pilot characterisation results.

Author contributions

A.Z. and A.H.D.H.: collection and assembling of the data, data analysis and interpretation, and manuscript writing. M.Ma.: collection and assembling of the data. M.D., R.M-D., P.B., K.R, M.J. and M.Mu.: Manuscript validation. M.P.: conception and design, data assembling, analysis and interpretation, manuscript writing.

Funding

This project was funded by EXO Biologics SA (Belgium) after agreement with the University of Padova, Department of Women's and Children's Health (Project N°: POZZ_COMM_23_02, PI: MP), by the Ministero dell'Università e della ricerca (MUR) with the project PRIN 2022 (POZZ_prin2022DM104.23_02) and supported by the DGO6 funding from the Wallonie Recherche SPW in Belgium (Grants No. 8358 and No. 8357).

Declarations

Competing interests

The authors declare no competing interests.

Consent for publication

All authors agree to publish the work.

Additional information

Supplementary Information The online version contains supplementary material available at https://doi.org/10.1038/s41598-025-24612-5.

Correspondence and requests for materials should be addressed to M.P.

Reprints and permissions information is available at www.nature.com/reprints.

Publisher's note Springer Nature remains neutral with regard to jurisdictional claims in published maps and institutional affiliations.

Open Access This article is licensed under a Creative Commons Attribution-NonCommercial-NoDerivatives 4.0 International License, which permits any non-commercial use, sharing, distribution and reproduction in any medium or format, as long as you give appropriate credit to the original author(s) and the source, provide a link to the Creative Commons licence, and indicate if you modified the licensed material. You do not have permission under this licence to share adapted material derived from this article or parts of it. The images or other third party material in this article are included in the article's Creative Commons licence, unless indicated otherwise in a credit line to the material. If material is not included in the article's Creative Commons licence and your intended use is not permitted by statutory regulation or exceeds the permitted use, you will need to obtain permission directly from the copyright holder. To view a copy of this licence, visit http://creativecommons.org/licenses/by-nc-nd/4.0/.

© The Author(s) 2025